Electrical Power and Energy Systems 141 (2022) 108264

Contents lists available at ScienceDirect

International Journal of Electrical Power and Energy Systems

journal homepage: www.elsevier.com/locate/ijepes

Faulty feeder detection based on fully convolutional network and fault trust degree estimation in distribution networks

Jiawei Yuan, Zaibin Jiao *

School of Electrical Engineering, Xi'an Jiaotong University, Xianning West Road No. 28, Xi'an 710000, China

ARTICLE INFO

Keywords:
Completeness
Fault trust degree estimation
Faulty feeder detection
Fully convolutional network
Interpretability

ABSTRACT

Faulty feeder detection is crucial to maintaining the safety and stable operation of power grids after single line-to-ground (SLG) faults occur in distribution networks. Existing detection methods have achieved good performance based on multi-feature fusion, but the extracted features commonly lack completeness and the detection process is poor in interpretability. This paper proposes a detection method based on fully convolutional network and fault trust degree estimation, which seeks to enhance its completeness and interpretability by mining the clear physical meaning from raw fault signals. Firstly, the zero-sequence current waveforms of all feeders were superimposed in the same plot to acquire the overall evaluation of fault conditions. Subsequently, a fully convolutional network was established to segment the waveforms of faulty feeder, suspected faulty feeder, and healthy feeders from the superimposed waveforms. Secondly, the segmented waveform of faulty feeder was compared with raw current waveforms, and an estimation method was introduced to quantitatively describe the fault trust degree of each feeder on the waveform scale, which is clear, complete, and intuitive. Finally, the faulty feeder can be detected after fault trust degree estimation. Various tests using PSCAD simulation, RTDS, field test, and practical fault data validate the efficiency of the proposed method.

1. Introduction

Since distribution systems with non-effective grounding are allowed to operate 1–2 h after occurrence of SLG faults, the non-effective grounding modes, such as ungrounded and resonant grounding, are extensively used in medium-voltage distribution networks [1]. Despite the reliability improvement in uninterrupted power supply, serious faults, such as interphase short, equipment damage, and casualties, may occur if the faulty feeders cannot be accurately identified and isolated. However, the SLG fault currents are weak, and fault transients are complex, especially for the resonant grounding networks, thereby posing great challenges for faulty feeder detection. Therefore, it is necessary to propose SLG faulty-feeder detection methods with high accuracy and reliability to enhance the safety and stable operation of distribution networks.

The existing faulty-feeder detection methods can be mainly divided into two categories: steady-state methods [2–7] and transient methods [8–16]. Fault characteristics of steady-state zero-sequence electrical parameters, such as amplitude, polarity, power, and admittance [2–4], are utilized to identify the faulty feeder. However, the steady-state methods have inherent limitations [5], especially for the resonant grounding networks and high impedance faults. Furthermore, in addition to the existing steady-state parameters, signal-injection methods [6–7] can realize faulty-feeder detection by tracking the certain injected signals, and they commonly require the assistance of additional devices, which would increase the construction costs and risks of devices damage.

Considering that transient components are several times larger than steady-state components after SLG faults, the transient methods usually extract rich transient fault features by using modern signal processing (MSP) algorithms, thus improving the detection accuracy. In [8], wavelet packet transform (WPT) is used to extract the decaying DC component, correlation component, and energy entropy component of zero-sequence currents, and the faulty feeder can be detected based on multi-feature fusion. In [9], Hilbert-Huang transform (HHT) is applied to decompose zero-sequence currents into several intrinsic mode functions (IMF), and the energy of the high-frequency IMFs is calculated to identify the faulty feeder. In [10], S-transform is adopted to get the spectral energy and differential energy, and microgrid protection is realized. Furthermore, wavelet transform (WT) [11–12], mathematical

* Corresponding author at: School of Electrical Engineering, Xi'an Jiaotong University, Xianning West Road No. 28, Xi'an 710000, China.
E-mail address: jiaozaibin@mail.xjtu.edu.cn (Z. Jiao).

https://doi.org/10.1016/j.ijepes.2022.108264
Received 23 January 2022; Received in revised form 30 March 2022; Accepted 11 April 2022
0142-0615/© 2022 Elsevier Ltd. All rights reserved.

morphology (MM) [13–14], and variational mode decomposition (VMD) [15–16], are also utilized in this field. Despite certain improvement on detection accuracy, the limiting factors that adversely affect the detection performance can be summarized as: 1) most MSP algorithms adopt fixed basis functions, which would result in low feature representation ability [17]; 2) the extracted features lack adequate completeness, and they cannot adapt to all fault scenarios; 3) the detection strategies based on multi-feature fusion or human experience are not optimal, and misjudgments may occur due to the failure of certain features.

To remedy the deficiency of the transient methods, machine learning (ML) algorithms has been introduced to further improve the detection accuracy. Since ML algorithms can adaptively learn and combine high-level features based on large amounts of fault data, the detection methods expect to have good performance by using ML algorithms. For instance, the fault features both in time domain and frequency domain are extracted by WT, and they are combined by convolutional neural network (CNN) [18]. IMFs of zero-sequence currents obtained by VMD are utilized as the input of long short-term memory neural network (LSTM), and the faulty feeder can be identified according to the output of LSTM [19]. In addition, neural network [20–21], clustering methods [22–23], and ensemble learning algorithm [24–25], are also employed as classifiers for detecting the faulty feeder. However, these ML-based methods have not been applied in practical distribution systems, and this is mainly because: 1) the extracted high-level features lack clear physical meaning; 2) the detection process has poor interpretability; 3) the generalization capability needs to be further verified when the detection methods encounter new fault scenarios.

To address the shortcomings of the existing methods, this paper proposes a novel detection method based on fully convolutional network (FCN) and fault trust degree estimation (FTDE), which has better performance in completeness of extracted features and interpretability of detection strategy. The main contributions are as the flowing:

1) Physical Meaning and Completeness of Extracted Features Can Be Enhanced: Raw zero-sequence current waveforms of all feeders are first superimposed in the same plot, and then an FCN is established to segment the waveform corresponding to the faulty feeder from the superimposed waveforms. Therefore, instead of extracting detailed features from raw fault currents, raw current waveforms are directly utilized to measure the fault degrees on the waveform scale. Since the raw waveforms have clear physical meaning and completeness, the proposed method has superior feature representation ability.

2) Interpretability of Detection Strategy Can Be Further Improved: From FCN aspect, the segmented results can be determined as detailed understanding on the superimposed waveforms, which corresponds to the raw current of each feeder. Besides, the segmented results are compared with raw current waveforms based on FTDE, and the detection strategy can be constructed, which is clear and intuitive. Therefore, FCN can directly exhibit the segmented results from raw superimposed waveforms, and FTDE can measure the fault degree of each feeder by comparing raw waveforms with the segmented results, which has strong interpretability.

The rest of the paper is organized as follows. Section 2 analyzes the existing detection methods in detail and points out their limitations and further improvement. Section 3 presents the detailed implementation process of the proposed method. The conducted case verifications are discussed in Section 4. Further, the PSCAD simulation, RTDS simulation, field test, and practical fault data are introduced along with some necessary analysis and comparisons. Finally, the study is concluded in Section 5.

2. Related works

Existing faulty-feeder detection methods can be classified into two groups, which can be called as “Method 1” and “Method 2” in this paper. The two methods are analyzed in this section, and their limitations and further improvement are detailed discussed.

2.1. Method 1

For Method 1, several fault features are extracted from raw fault signals using MSP algorithms, and the extracted features are employed to construct the detection schemes based on different strategies, as shown in Fig. 1. Since the fault transients are complex and fault scenarios are varied, Method 1 can improve the detection accuracy by extracting efficient fault features and constructing suitable strategies.

For instance, transient energy, kurtosis, and cross-correlation distance are extracted from zero-sequence currents, and they are combined based on multiple evidence fusion method [26], where the feeder corresponding to the maximum fusion result is determined as the faulty feeder. Similarly, the steady-state components of zero-sequence currents are calculated to construct the criterion 1, the transient components are obtained to serve as the criterion 2, and the two criterions are selected by the threshold judgment [27]. Therefore, Method 1 expects to extract and combine several fault features with certain physical meaning, which can reflect the fault degrees of raw signals.

However, there are two main drawbacks: 1) the extracted fault features can only reflect characteristics of raw signals in some aspects, which lacks adequate completeness. Besides, the MSP algorithms may obtain the fault features without physical meaning in the extraction process [17]; 2) the performance of the constructed schemes relies heavily on fusion theory or human experience, which would not always achieve the optimal detection results. Therefore, the completeness and detection strategies of Method 1 can be further improved.

2.2. Method 2

For Method 2, ML algorithms are commonly utilized as tools for constructing the detection strategies, as shown in Fig. 2. The core of Method 2 is the selection of input features and ML algorithms. For the input features, they can be either extracted by MSP algorithms or adaptively learned by ML algorithms. For the ML algorithms, different models, such as neural network, support vector machine (SVM), and ensemble learning, can be utilized to combine the input features and output the detection results.

For instance, current waveform energy and normalized joint time-frequency moments are extracted as fault features, and SVM is used as a classifier for detection [28]. In [29], the sampled data of zero-sequence currents are directly employed as the input of the 1-D CNN, which can adaptively learn the fault features from raw currents, and the CNN is utilized as a tool both for feature extraction and feature fusion. These methods require large amounts of data for training and achieve good detection performance in simulations.

Despite certain improvement in detection accuracy compared with Method 1, the factors hindering the application prospects of Method 2 are as follows: 1) the extracted features are high-level features in the aspects of ML algorithms, which lacks clear physical meaning; 2) the process of feature fusion is data-driven, which is poor in interpretability. Therefore, the physical meaning and interpretability of Method 2 are the limiting factors for future practical applications.

In summary, a desirable faulty-feeder detection method should have good performance in the following aspects: clear physical meaning, completeness, interpretability, and suitable detection strategy.

3. Proposed method

3.1. Proposed detection framework

In this paper, an FCN-FTDE based faulty-feeder detection scheme is proposed. The proposed scheme comprises four modules: 1) current waveform procession and superimposition; 2) image creation; 3) waveform segmentation; 4) fault trust degree estimation. The simplified diagram of the detection scheme is exhibited in Fig. 3.

Firstly, raw zero-sequence currents are superimposed in the same

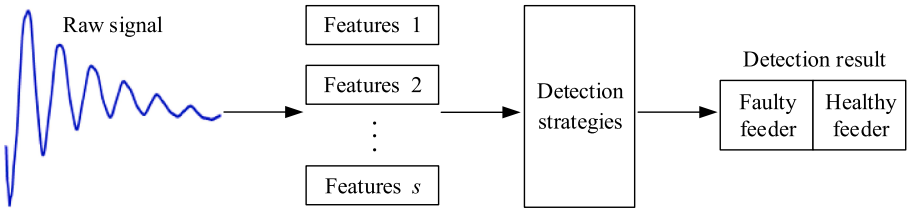

Fig. 1. Diagram of Method 1. If the raw signal is corresponding to the faulty feeder, the detection result is the faulty feeder, otherwise, the detection result is healthy feeder.

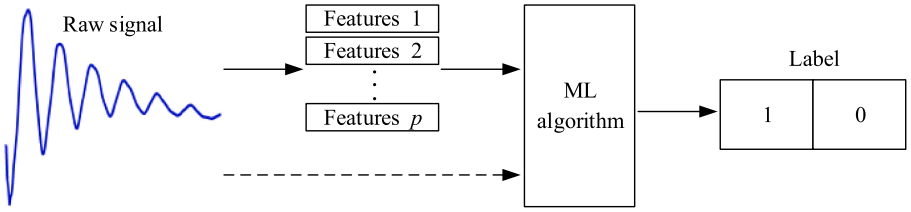

Fig. 2. Diagram of Method 2. If the raw signal is corresponding to the faulty feeder, the output label is '1', otherwise, the output label is '0'.

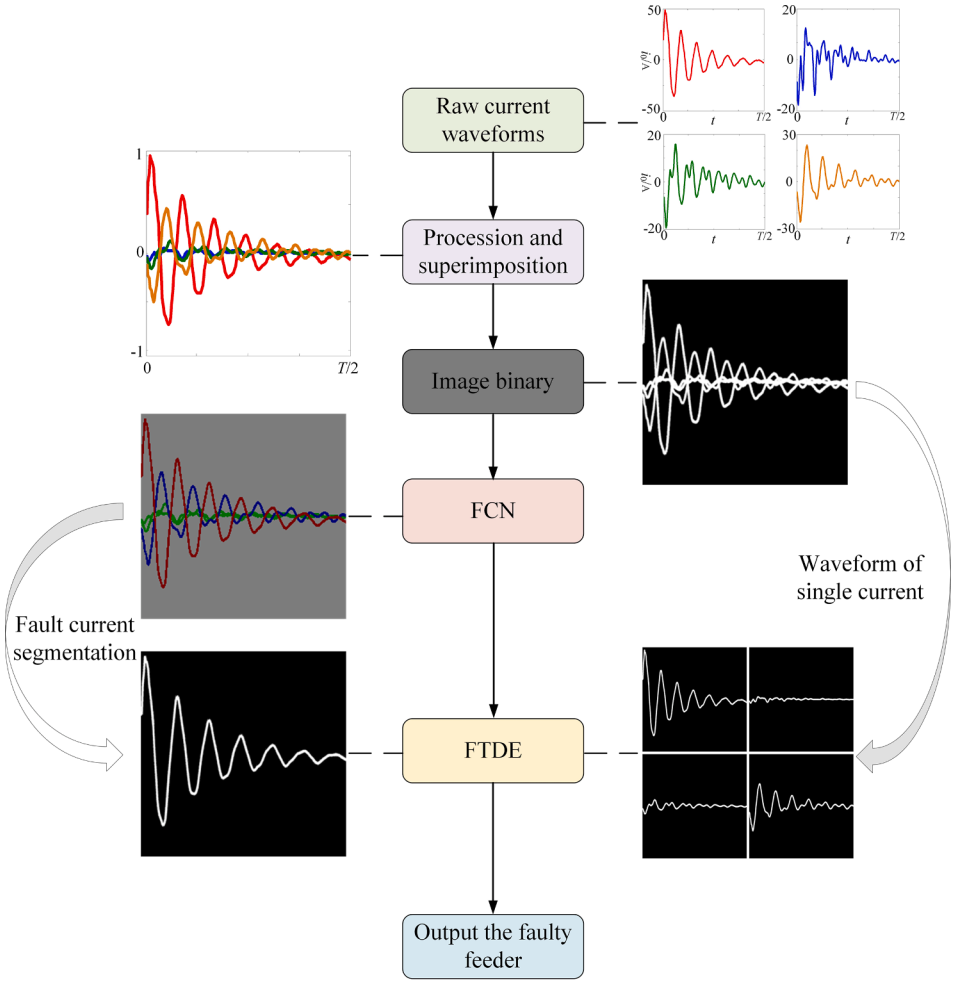

Fig. 3. The diagram of the proposed detection scheme. (Take the zero-sequence currents in a distribution network composed of four feeders as an example).

plot, and the overall perspective of the SLG fault can be reflected. Secondly, the binary image composed of currents of all feeders is generated. Subsequently, the generated image is input to the FCN, which can segment different current waveforms with different meanings. Finally, FTDE can be conducted between the segmented waveform corresponding to the faulty feeder and raw current waveform of each feeder, and

the faulty feeder can be detected based on the estimation result.

Compared with Method 1 and Method 2, the proposed method has superior performance in the following aspects:

1. From the aspect of physical meaning: The superimposed current waveforms of all feeders are segmented into waveforms with different meanings based on FCN, including the waveform of the faulty feeder, suspected feeder, and healthy feeders. That is to say, the output of FCN has clear physical meaning, which can be easily associated with raw zero-sequence currents.
2. From the aspect of completeness: the target of feature extraction is the whole waveform, rather than specific fault features. Since the whole waveform has the complete fault features, the proposed method can satisfy the requirement for completeness, which is no longer limited to certain features.
3. From the aspect of interpretability: compared with the output label of Method 2, which is directly corresponding to the final detection result, FCN is first utilized to segment the superimposed waveforms into waveforms with different meanings, rather than a mere data-driven fusion tool. Among them, FCN attempts to realize detailed understanding based on classifying each pixel in the image generated by superimposed waveforms. Subsequently, the final faulty-feeder detection result depends on the FTDE between the segmented results and raw current waveforms, and the detection process is clear and intuitive.
4. From the aspect of detection strategy: the proposed FTDE with clear physical meaning and interpretability can better measure the fault degree on the waveform scale. Therefore, the detection strategy based on FTDE is simple, practical, and effective.

The detailed implementation is further illustrated in the following section.

3.2. Waveform processing and image creation

The first half-cycle zero-sequence current of each feeder is sampled after SLG faults, and the maximum absolute values of currents are calculated using (1).

$$i_M(n) = Max(|i_n(t)|)\ ,\quad n \in [1,N],\ t \in [0,\frac{T}{2}] \tag{1}$$

where T is the cycle of zero-sequence current, N is the number of feeders, $i_n(t)$ is the raw zero-sequence current of n-th feeder, and $i_M(n)$ is the maximum absolute values of n-th feeder.

Subsequently, raw sampled current of n-th feeder is normalized using (2).

$$i_n^{'}(t) = i_n(t) \times \frac{i_M(n)}{(Max(i_M(n)))^2}\ ,\quad n \in [1,N],\ t \in [0,\frac{T}{2}] \tag{2}$$

where i'_n(t) is the normalized current of n-th feeder.

Considering the loss of fault characteristics caused by normalization, it is necessary to enlarge the amplitude of the zero-sequence current using η, shown in (3), whose amplitude ($i'_M(n)$) is the second largest.

$$\eta = \frac{Max(i_M^{'}(n))}{Second\_Max(i_M^{'}(n))},\quad n \in [1,N] \tag{3}$$

where $Max(i'_M(n))$ is the maximum amplitude of the currents, and $Second\_Max(i'_M(n))$ is the second largest amplitude.

If η is greater than two, the current amplitude of the feeder with second largest amplitude will be enlarged by $\eta/2$; otherwise, it will remain at the raw amplitude.

Subsequently, the processed current waveforms of all feeders are superimposed in the same image. The generated image contains the completed features of raw fault currents, laying the foundation for further faulty-feeder detection. Finally, the binary processing of the image is conducted, and the image is resized to 256 × 256.

3.3. Waveform segmentation

Semantic segmentation lays important foundation for detailed image understanding, which is extensively used in autonomous driving, medicine, and geography [30]. As the sate-of-the-art method in the field of semantic segmentation, FCN [31] has achieved successful applications. Compared with traditional CNN, FCN converts the last fully connected (FC) layers into convolutional layers, and the feature map is finally returned to an image with the same size as the raw image based on upsampling operations. Besides, skip structures are added into the network to fuse outputs of different layers, which leads to high quality segmentation results.

FCN mainly contains convolutional layer, max-pooling layer, upsampling layer, and fusion layer. Wherein, the convolution layer and max-pooling layer are alternately stacked for feature extraction in the encoding stage, and the upsampling layer and fusion layer are alternately stacked for semantic segmentation in the decoding stage. The convolution process can be described as follows:

$$x_j^l = f(\sum_t k_{t,j}^l * x_t^{l-1} + b_j^l) \tag{4}$$

where x_j^l denotes the output of j^{th} filter in the l^{th} convolutional layer, and x_t^{l-1} denotes the output of t^{th} feature map in the $(l-1)^{\text{th}}$ convolutional layer. $k_{t,j}^l$ denotes the learned weights of j^{th} filter in the l^{th} convolutional layer, and b_j^l is the bias term. f (.) denotes the non-linear activation function.

Subsequently, the max-pooling layer is utilized to reduce the learning parameters and avoid over-fitting, and it can be expressed as follows:

$$p_j^l = \underset{r \in M_j}{max}\left(x_j^l(r)\right) \tag{5}$$

where p_j^l denotes the output of j^{th} filter in the l^{th} max-pooling layer, and M_j is the area of pooling operation.

Since the size of feature maps is reduced after max-pooling operation, the upsampling operation is utilized in the decoding stage as follows:

$$u_j^k = g\left(p_j^l\right) \tag{6}$$

where u_j^k denotes the output of j^{th} filter in the k^{th} upsampling layer, and g (.) denotes the upsampling function.

To fuse outputs of different layers, fusion layer is conducted:

$$y_j^k = p_j^{l-1} + u_j^k \tag{7}$$

where y_j^k denotes the output of j^{th} filter in the k^{th} fusion layer, p_j^{l-1} denotes the output of j^{th} filter in the $(l-1)^{\text{th}}$ max-pooling layer, where p_j^{l-1} has the same size as u_j^k.

In this paper, the established FCN with detailed parameters is shown in Fig. 4, and the filters in the encoding stage are 64, 64, 64, 128, and 128, respectively.

To realize detailed understanding of superimposed current waveforms, it is necessary to classify waveforms into different types, including the waveforms of the faulty feeder, suspected faulty feeder, and healthy feeders. In fact, images are composed of pixels, and the binary images of current waveforms consists of element 1 and element 0, where the white color in the images corresponds to the element 1 and the black denotes the element 0. Since the images input to the established FCN have the same size as the output images, the detection results

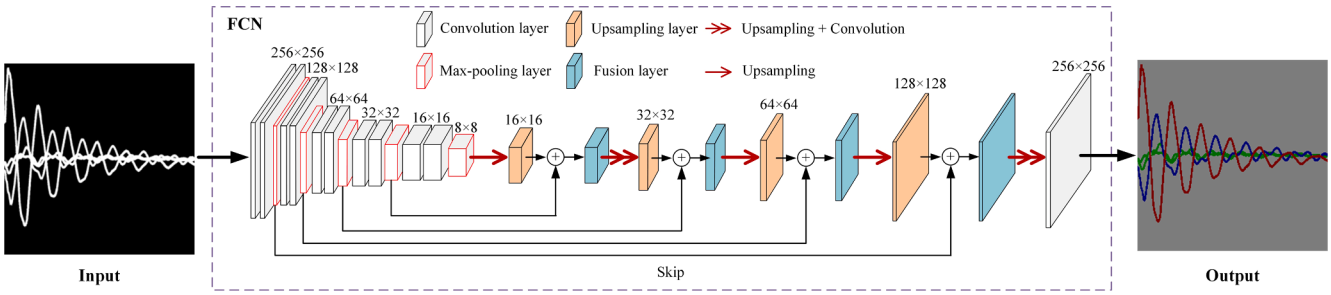

Fig. 4. Structure of FCN.

of FCN can be deemed as pixelwise prediction, which implies that each pixel of the input images would be labeled with the corresponding class. That is to say, the FCN would make a class prediction at every pixel, and totally four classes are determined in this paper. Among them, the class 'faulty feeder' in the output images is depicted as red, the class 'suspected faulty feeder' is exhibited as blue, and the class 'healthy feeders' and 'background' is green and grey, respectively, as shown in Fig. 4. Finally, all red pixels can be considered as the waveform of the faulty feeder, and all blue pixels and green pixels correspond to the waveform of the suspected faulty feeder and healthy feeders, respectively. Compared with other ML-based methods, the outstanding advantage of the FCN-based method lies that its output has clear physical meaning, and the final detection results would depend on further fault trust degree estimation, not just the single output label of ML algorithms.

3.4. Fault trust degree estimation

Since FCN can segment the current waveform of the faulty feeder, it is necessary to measure the fault degree of each feeder on the waveform scale. That is to say, the segmented waveform of the faulty feeder needs to be compared with raw waveform of each feeder, which can further improve the interpretability. Considering that dice coefficient can measure the similarity between two sets, FTDE is conducted as follows:

$$Dice_i(X_i, Y) = \frac{2|X_i \cap Y|}{|X_i| + |Y|} \tag{8}$$

where X_i denotes the set of the binary image generated by the i-th feeder current, and Y denotes the set of segmented waveform corresponding to the faulty feeder. $\cap$ denotes the intersection set between X_i and Y, and $Dice_i$ is the calculated dice coefficient of the i-th feeder.

Finally, the detection strategy can be constructed: the feeder whose dice coefficient is larger than 0.5 is determined as faulty feeder, and the feeder whose dice coefficient is smaller than 0.5 is the healthy feeder. Further, if the dice coefficients of all feeders are smaller than 0.5, the fault type can be identified as bus fault. Evidently, the proposed detection strategy is based on the fault degree estimation from the aspect of raw waveforms, which has clear physical meaning and interpretability.

3.5. FCN training

Considering the difficulty for collecting the actual fault data, three training models are established using PSCAD to simulate SLG faults that occur in feeders and buses. The structure of simulation models is shown in Fig. 5. The parameters concerning the overhead lines are as follows: $R_1 = 0.17\ \Omega$/km, $L_1 = 1.21$ mH/km, $C_1 = 0.0097\ \mu$F/km, $R_0 = 0.23\ \Omega$/km, $L_0 = 5.48$ mH/km, and $C_0 = 0.006\ \mu$F/km. Likewise, the parameters concerning the cable lines include $R_1 = 0.098\ \Omega$/km, $L_1 = 0.274$ mH/km, $C_1 = 0.351\ \mu$F/km, $R_0 = 0.246\ \Omega$/km, $L_0 = 0.955$ mH/km, and $C_0 = 0.166\ \mu$F/km. The sampling frequency is 20 kHz. Furthermore, different fault locations, fault time, and fault impedances are considered in the data-production processes, and the detailed fault scenarios are summarized in Table 1.

For SLG faults occurred in feeders, the ground truths corresponding to the generated binary images can be determined as: the red color corresponds to the waveform of the faulty feeder, the blue color corresponds to the waveform of the healthy feeder with maximum amplitude (called as suspected faulty feeder), the green color corresponds to the waveform of the remaining healthy feeders, and the grey color

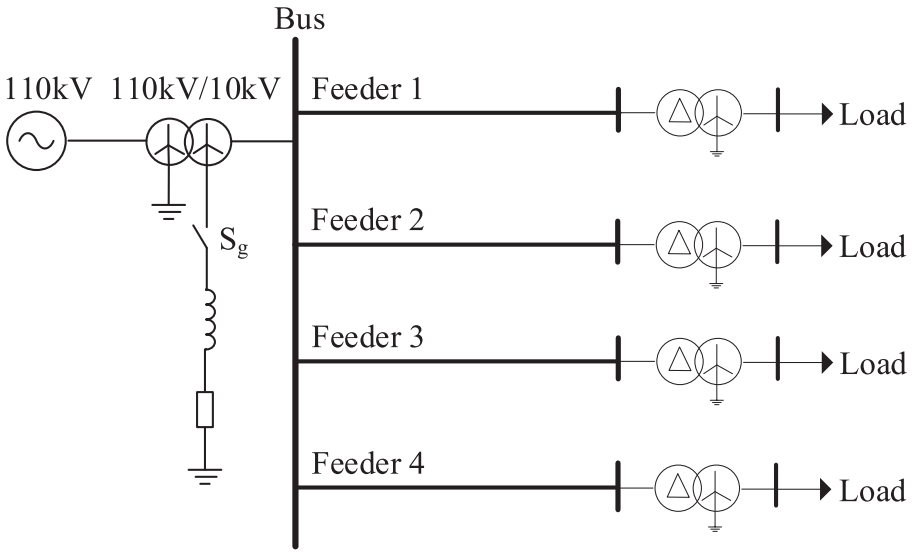

Fig. 5. PSCAD model of the established distribution system in training dataset.

Table 1
Parameters and fault scenarios in training set.

PSCAD Simulation		Training Samples		
Parameters	Model	Training model 1	Training model 2	Training model 3
	Grounding mode	Compensation system	Compensation system	Ungrounded system
	Compensation degree	8%	8%	/
	Feeder type	Overhead	Cable / Overhead	Overhead
	Length (km)	10 / 20 / 30 / 40	Cable:10 / 20, Overhead: 30 / 40	10 / 20 / 30 / 40
Scenariors	Fault location	10% / 50% / 90% / Bus		
	Initial phases	0°~360° per 22.5°(Line fault) / 0°~360° per 1.8°(Bus fault)		
	Grounding resistances	20 Ω / 100 Ω / 500 Ω / 1000 Ω		
Sample Number	Simulation data	816 (Line fault) / 804 (Bus fault)	816 (Line fault) / 804 (Bus fault)	816 (Line fault) / 804 (Bus fault)
	Image	2448 (Line fault)		2412 (Bus fault)

corresponds to the background. Regarding the bus fault, there is no waveform corresponding to the faulty feeder, and two waveforms of the healthy feeders are labeled as blue color.

It is noteworthy that the training dataset is easy to obtain by using PSCAD simulation. Besides, to verify the strong generalization capability of the proposed method, complex fault scenarios, such as arc grounding faults, nonlinear high impedance faults, and single-phase line-broken faults, are not considered in the training dataset, while they are directly used to test its detection performance in the test process.

4. Case study

To verify the generalization capability and application prospects of the proposed method, large amounts of fault data were collected from different distribution networks. Among them, 13,120 sets of SLG fault data acquired from PSCAD simulation, 69 sets of recorded data generated from RTDS hardware-in-the-loop (HIL) test system, 36 sets of field data generated from field test, and 12 sets of practical fault data in real distribution systems were collected in the following test. Among them, the topologies, parameters, feeder types, and fault conditions in these distribution networks were completely different from those in the training dataset. Notably, both fault data in RTDS HIL test, field test, and practical data test was collected from practical fault recorders, considering real measurement errors and noise interference.

4.1. PSCAD simulation

To obtain sufficient fault data utilized for performance evaluation, a 10-kV distribution network is established by using PSCAD simulation, as shown in Fig. 6, considering different neutral grounding modes, varied parameters, and extreme fault conditions. Wherein, the neutral grounding modes can be changed through switch S_g, and the network are composed of overhead lines, cable lines, and hybrid lines, leading to more complex fault transients. Besides, the sampling frequency in PSCAD simulation is just 5 kHz, which is significantly lower than that in the training dataset, and the low sampling frequency can be easily realized in practical applications. Furthermore, Gaussian white noise with the signal-to-noise-ratio (SNR) of 30 dB was added to each sampled zero-sequence current. The detailed parameters and fault conditions are summarized in Table 2 and Table 3, respectively.

Typical binary images and the corresponding segmentation results under different fault conditions are shown in Fig. 7. Among them, the x-axis in images represents the sampling time (first half-cycle of currents), and the y-axis represents the normalized amplitude ([-1, 1]).

It can be seen that there are changing fault characteristics of zero-sequence currents under different fault conditions. Among them, since the faulty-feeder current has larger amplitudes and different polarities compared to the healthy-feeder currents along the whole time axis, it is relatively easy to distinguish the faulty feeder from healthy feeders in the non-grounding network. Whereas, the faulty-feeder current would be affected by the inductance current flowing through the extinction coil in the resonant grounding network, and the transient zero-sequence currents would decay rapidly especially under high resistance grounding faults, which makes it rather difficult for identifying the faulty feeder. However, the established FCN can still find the waveform

Table 2
Parameters of feeders in test set.

Type	Phase-sequence	R (Ω/km)	L (mH/km)	C (μF/km)
Overhead line	Positive-sequence	0.33	1.31	0.007
	Zero-sequence	1.04	3.96	0.004
Cable line	Positive-sequence	0.079	0.26	0.373
	Zero-sequence	0.23	0.93	0.166

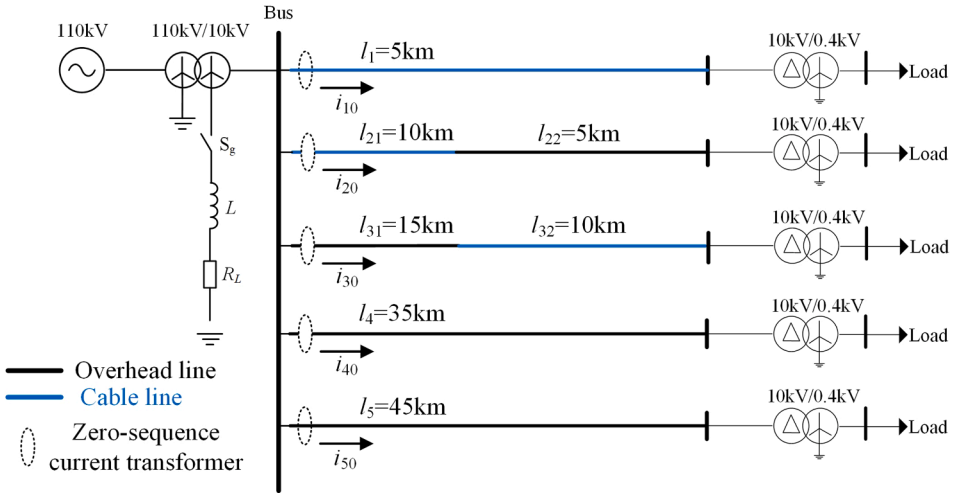

Fig. 6. PSCAD model of 10-kV distribution network in test set.

Table 3
Fault scenarios in test set.

PSCAD Simulation		Parameters	
Scenariors	S_g	Open	Closed
	Fault location	5% / 35% / 85%, Bus	
	Initial phases	0°–360°, per 9°	
	Grounding resistances	1 Ω / 40 Ω / 120 Ω / 470 Ω / 620 Ω /1.3 kΩ / 2 kΩ / 5 kΩ / 8 kΩ / 10 kΩ	
Sample number		6150 (line fault)/410 (bus fault)	6150 (line fault)/410 (bus fault)

of the faulty feeder with high reliability under different fault scenarios, and the corresponding dice coefficients under line faults are 0.89, 0.90, 0.80, 0.78, 0.79, and 0.80, respectively, and the dice coefficient of each feeder in Fig. 7 (d) and Fig. 7 (h) is smaller than 0.5. Obviously, the proposed method can not only detect the faulty feeder, but also has good interpretability and robustness.

Furthermore, the detection performance of the proposed method is compared with the method [26] and method [33]. The detailed detection results are shown in Table 4, and the symbol '×' means that the method is not applicable under the corresponding conditions. Among them, the method [26] constructed the detection scheme based on the multiple feature fusion of transient energy, kurtosis, and cross-correlation distance (CCD), and the method [33] selected the faulty feeder based on the change of current share (CCS) and the difference between CCS (DCCS).

As shown in Table 4, the method [26] has 100% detection accuracy for line faults in the non-grounding network, while it has poor detection performance in the resonant grounding network. This is mainly because the extracted fault features are susceptible to the transient processes due to the compensation of extinction coil. For example, the zero-sequence currents have rich high-frequency components, as shown in Fig. 7 (e), and the faulty-feeder current has significantly larger transient energy

Table 4
Detection accuracy in PSCAD simulation.

S_g	Fault type	Paper [26]	Paper [33]	Proposed method
Open	Line fault	100%	×	**100%**
	Bus fault	×	×	**98.54%**
Closed	Line fault	75.11%	94.21%	**99.37%**
	Bus fault	×	14.63%	**99.76%**

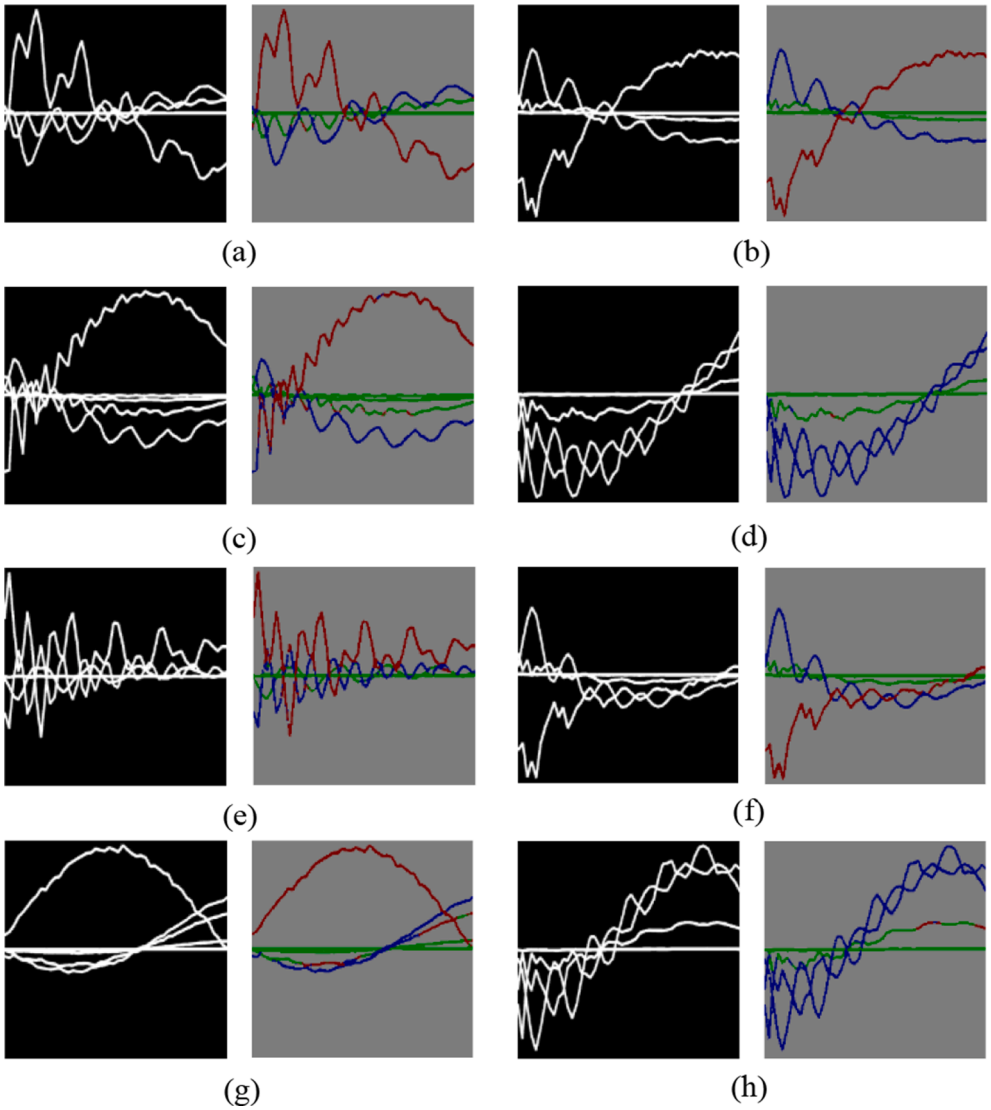

Fig. 7. Raw binary images and the corresponding segmentation results in PSCAD simulations (a) fault in feeder 1, 0.25 km, 27°, 1 Ω, S_g is open; (b) fault in feeder 2, 12.75 km, 261°, 120 Ω, S_g is open; (c) fault in feeder 4, 29.75 km, 0°, 10 kΩ, S_g is open; (d) fault in Bus, 72°, 5 kΩ, S_g is open; (e) fault in feeder 1, 0.25 km, 27°, 1 Ω, S_g is closed; (f) fault in feeder 2, 12.75 km, 261°, 120 Ω, S_g is closed; (g) fault in feeder 4, 29.75 km, 0°, 10 kΩ, S_g is closed; (h) fault in Bus, 72°, 5 kΩ, S_g is closed.

and CCD than healthy-feeder currents, thus making it easy for identifying the faulty feeder. However, the high-frequency components decay sharply in Fig. 7 (f), and the judgment of the initial extremum value for calculating CCD is easily affected by the oscillations, which results in lower transient energy and CCD in the faulty feeder. Finally, the failure of two of the three extracted features inevitably causes misjudgment for faulty-feeder detection. Furthermore, the feeder corresponding to the maximum fusion results is selected as the faulty feeder directly, which makes it unsuitable for identification of bus fault.

For the method [33], it has relatively high detection accuracy in the resonant grounding network, while it cannot adapt to faulty-feeder detection in the non-grounding network as it detects the faulty feeder based on the compensation characteristic of extinction coil. Furthermore, the threshold of DCCS for distinguishing line fault and bus fault is determined according to experience, which leads to poor performance in identification of bus fault in the established network.

In contrast, the proposed method not only has 100% faulty-feeder detection accuracy in the non-grounding network, but also has a high detection accuracy in the resonant grounding network. Besides, bus fault can also be identified with high reliability. Therefore, the proposed method has superior adaptability and strong generalization capability.

4.2. RTDS HIL test

The RTDS-based HIL test system is commonly utilized to test the performance of relay protection devices before they are put into practice. To verify the adaptability of the proposed method, the RTDS model is designed, as shown in Fig. 8.

The established network contains two grounding modes, including neutral point ungrounded and neutral point resonant grounding, and 15 feeders are connected to two Buses. Furthermore, the feeder parameters and fault scenarios used in RTDS simulation are summarized in Table 5, and the sampling frequency is 12 kHz.

As shown in Table 5, different feeders have varied parameters, and SLG faults with changing initial phases and grounding resistances are considered. Besides, since SLG faults are usually accompanied with arc grounding events, arc grounding faults are simulated by using Mayr arc model [32]. Typical binary images and the corresponding segmentation results are shown in Fig. 9, where the meanings of x-axis and y-axis are same as that in Fig. 7.

Evidently, the zero-sequence currents differ significantly under different fault conditions, which results in varied characteristics of oscillations and attenuation. Besides, zero-sequence currents may have certain distortions when SLG faults with arc grounding events occur, as shown in Fig. 9 (a), Fig. 9 (f), and Fig. 9 (g).

Despite these unfavorable conditions, the established FCN can still segment the waveform of the faulty feeder, and the corresponding dice coefficients are as follows: 0.89, 0.92, 0.83, 0.73, 0.91, 0.85, and 0.87, and the dice coefficient of each feeder in Fig. 9 (h) is smaller than 0.5. Thus, the proposed method can accurately detect the faulty feeder, and the detection process is clear, intuitive, complete, and effective.

The detailed detection results of the three methods are shown in Table 6, and the symbol '×' means that the method is not applicable under the corresponding conditions.

As shown in Table 6, both methods can accurately detect the faulty feeder when SLG faults occur in RTDS model 2 under different fault conditions, which demonstrates the efficiency for faulty-feeder detection in the resonant grounding distribution networks. However, the method [26] cannot identify the bus fault, and the method [33] cannot be applied to ungrounded distribution networks. In contrast, the proposed method can identify the bus fault and line fault, and it can also adapt to distribution networks with different grounding modes, which has broad adaptability.

4.3. Field test

Field test was conducted in the 10 kV distribution network of Luohe substation, Henan, China, and the network structure is shown in Fig. 10.

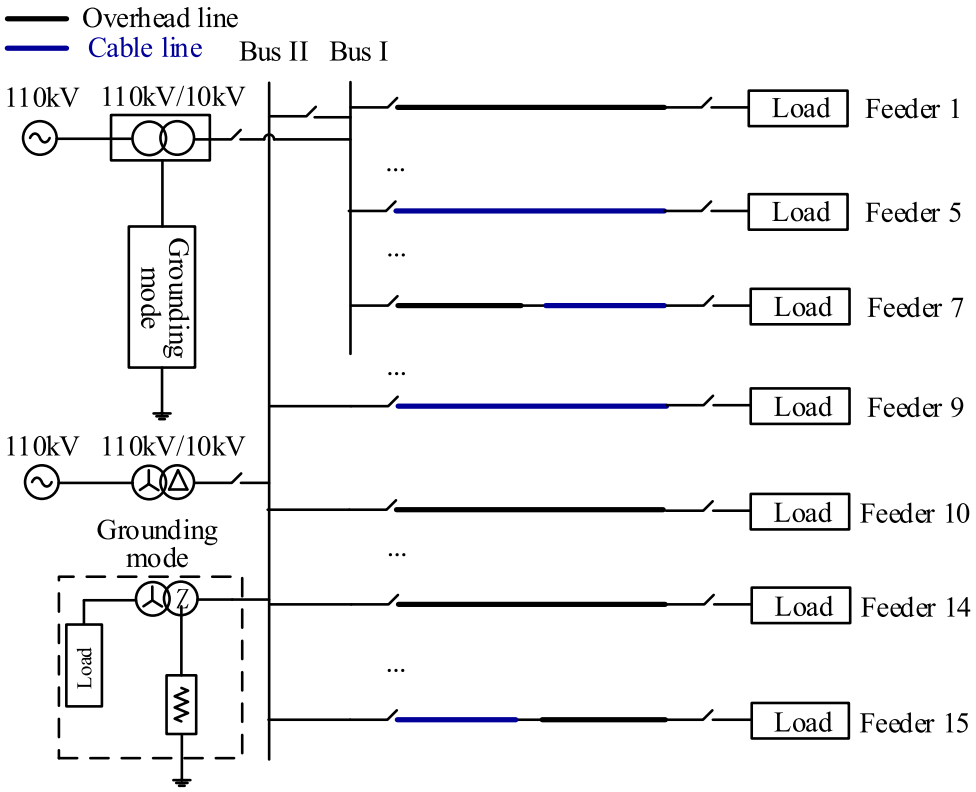

Fig. 8. RTDS model of 10-kV distribution system.

Table 5
Parameters and fault scenarios in RTDS simulation.

RTDS Simulation		Test Samples					
Parameters	Type	Overhead line			Cable line		
	Phase-sequence	R(Ω/km)	L(mH/km)	C(μF/km)	R(Ω/km)	L(mH/km)	C(μF/km)
	Positive- sequence	0.33 / 0.45	1.305 / 1.305	0.007 / 0.0068	0.0791 / 0.098	0.264 / 0.274	0.373 / 0.351
	Zero-sequence	1.041 / 1.443	3.963 / 4.046	0.004 / 0.0039	0.2273 / 0.2462	0.926 / 0.955	0.166 / 0.166
Scenarios	Model	RTDS model 1			RTDS model 2		
	Grounding mode	Ungrounded system			Compensation system		
	Faulted location	L1 / L5 / L7 / L9 / Bus			L1 / L5 / L7 / L9 / L10 / Bus		
	Initial phases	30°/ 90°/ 120°/ 123°/ 150°/ 180°/ 210°/ 270°/ 330°			30°/ 60°/ 90°/ 123°/ 150°/ 210°/ 243°/ 270°/ 330°		
	Grounding resistances	1.1 Ω / 5.82 Ω / 10 Ω / 1000 Ω			1.1 Ω / 10 Ω / 240 Ω / 1000 Ω		
	Unbalance voltage	0 V / 2.68 V / 5.67 V			0 V / 2.68 V / 5.67 V		
	Arc grounding	Yes / No			Yes / No		
Sample number		31			38		

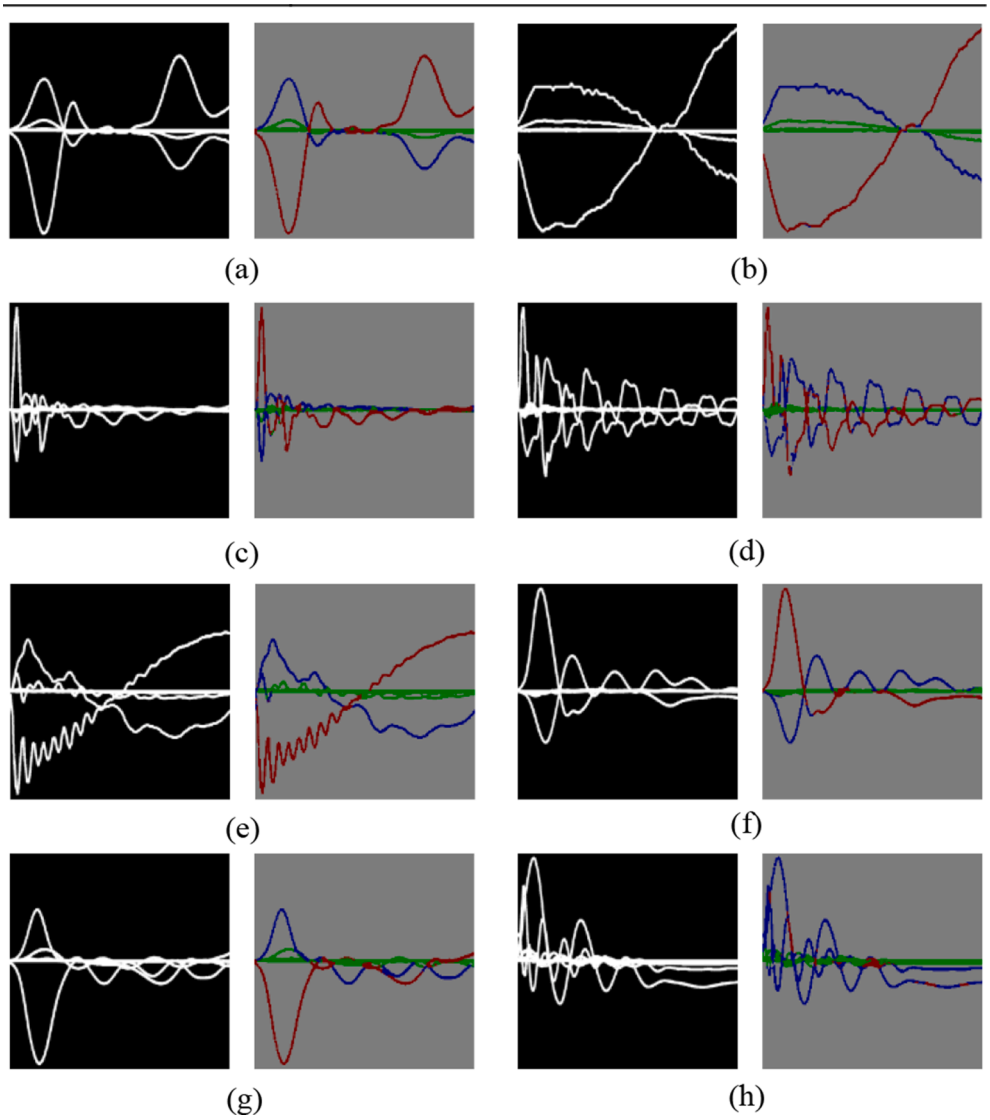

Fig. 9. Raw binary images and the corresponding segmentation results in RTDS simulations (a) fault in feeder 1, Bus I, 150°, 10 Ω, Arc, RTDS Model 1; (b) fault in feeder 1, Bus I, 180°, 1000 Ω, RTDS Model 1; (c) fault in feeder 5, Bus I, 123°, 10 Ω, RTDS Model 1; (d) fault in feeder 9, Bus II, 123°, 10 Ω, RTDS Model 1; (e) fault in feeder 5, Bus I, 150°, 1000 Ω, RTDS Model 2; (f) fault in feeder 5, Bus I, 123°, 10 Ω, Arc, RTDS Model 2; (g) fault in feeder 9, Bus II, 243°, 10 Ω, Arc, RTDS Model 2; (h) fault in Bus I, 60°, 10 Ω, RTDS Model 2.

Table 6
Detection accuracy in RTDS simulations.

Model	Fault type	Paper [26]	Paper [33]	Proposed method
RTDS model 1	Line fault	100%	×	**100%**
	Bus fault	×	×	**100%**
RTDS model 2	Line fault	100%	100%	**100%**
	Bus fault	×	100%	**100%**

In Fig. 10, there are six feeders, where feeders 1–3 are the practical feeders and feeders 4–6 are the analog feeders, and the grounding modes can be changed through grounding transformers. Specifically, the feeder 1 and feeder 2 are the overhead lines, which can be connected by the switch S_1, and feeder 3 is the cable line, which can be converted into a hybrid line through switch S_2. Furthermore, the capacitances of feeders 4–6 can be set to simulate distribution networks with different capacitive currents, where both symmetrical and asymmetric feeders can be

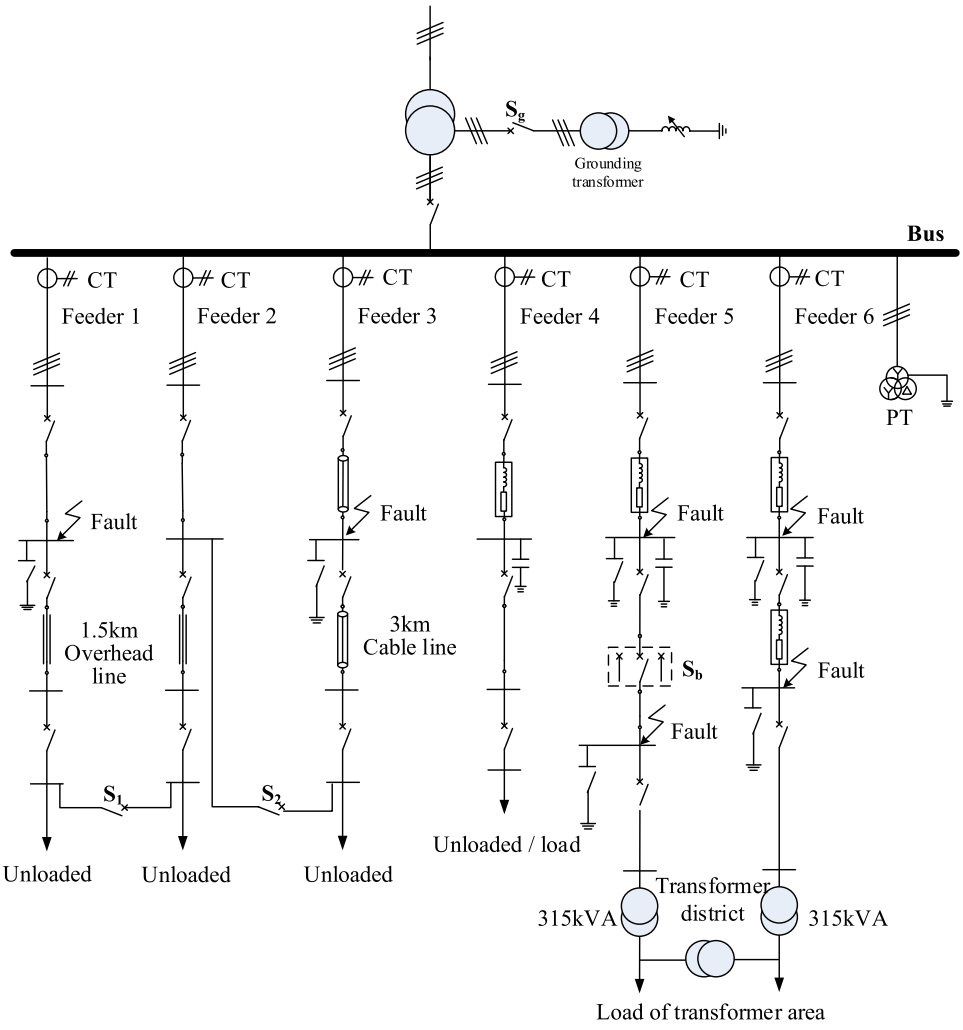

Fig. 10. Structure of the field test.

simulated, and feeder 5 can simulate single-phase line-broken faults.

Since SLG fault scenarios are varied in practical distribution networks, SLG faults occurred under different fault grounding types during field test, such as metal grounding, resistance grounding, arc grounding, and line-broken grounding. Among them, arc conditions with different discharge distances can be simulated through setting the discharge gap, and short gap discharge can be simulated when SLG faults occur in the practical cable line. Several binary images generated by the recorded waveforms and the corresponding segmentation results are shown in Fig. 11, where the meanings of x-axis and y-axis are same as that in Fig. 7.

As shown in Fig. 11, compared with zero-sequence currents in the RTDS simulation, the fault transients are more complex in field test, especially for arc grounding faults, where the zero-sequence currents have significant nonlinear distortions at the zero-crossing point. Furthermore, it is rather difficult to identify the faulty feeder due to small fault current when high impedance faults occur in the resonant grounding system, as shown in Fig. 11 (g) and Fig. 11 (h). These unfavorable conditions may cause great challenges for faulty-feeder detection. However, the established FCN can still segment the waveform of the faulty feeder, and the corresponding dice coefficients are as follows: 0.80, 0.73, 0.58, 0.88, 0.86, 0.84, 0.92, and 0.89. Thus, the proposed method still has good detection accuracy.

Totally 36 sets of fault data are collected in field test under sampling frequency 20 kHz, where 18 sets of fault data are recorded from the ungrounded system and the remaining data are recorded from the resonant grounding system. The detection results are shown in Table 7.

Notably, the method [26] has poor performance for faulty-feeder detection in the resonant grounding system. This is mainly because two of the three extracted features (energy, kurtosis, and cross-correlation distance) would fail under certain fault conditions, which inevitable results in misjudgments for the method [26] based on multi-feature fusion. For instance, the extracted energy and kurtosis of the faulty feeder are smaller than that of the healthy feeder under high impedance faults, as shown in Fig. 11 (g) and Fig. 11 (h), thus causing misjudgments of faulty-feeder detection. This indicates that the completeness of extracted features and efficiency of detection strategy are the inherent limitations for improving the detection accuracy. Furthermore, the method [33] can accurately detect the faulty feeder in the resonant grounding system, while it cannot realize detection in the ungrounded system. Compared with the two methods, the proposed method has 100% detection accuracy under all fault conditions in field test, which demonstrates its strong adaptability and generalization capability.

4.4. Practical data test

To verify the application prospects of the proposed method, 12 sets of practical SLG fault data sampled with 12 kHz are collected from the Chenzhou, Shaoyang, and Xi'an substations in 2020. Among them, the

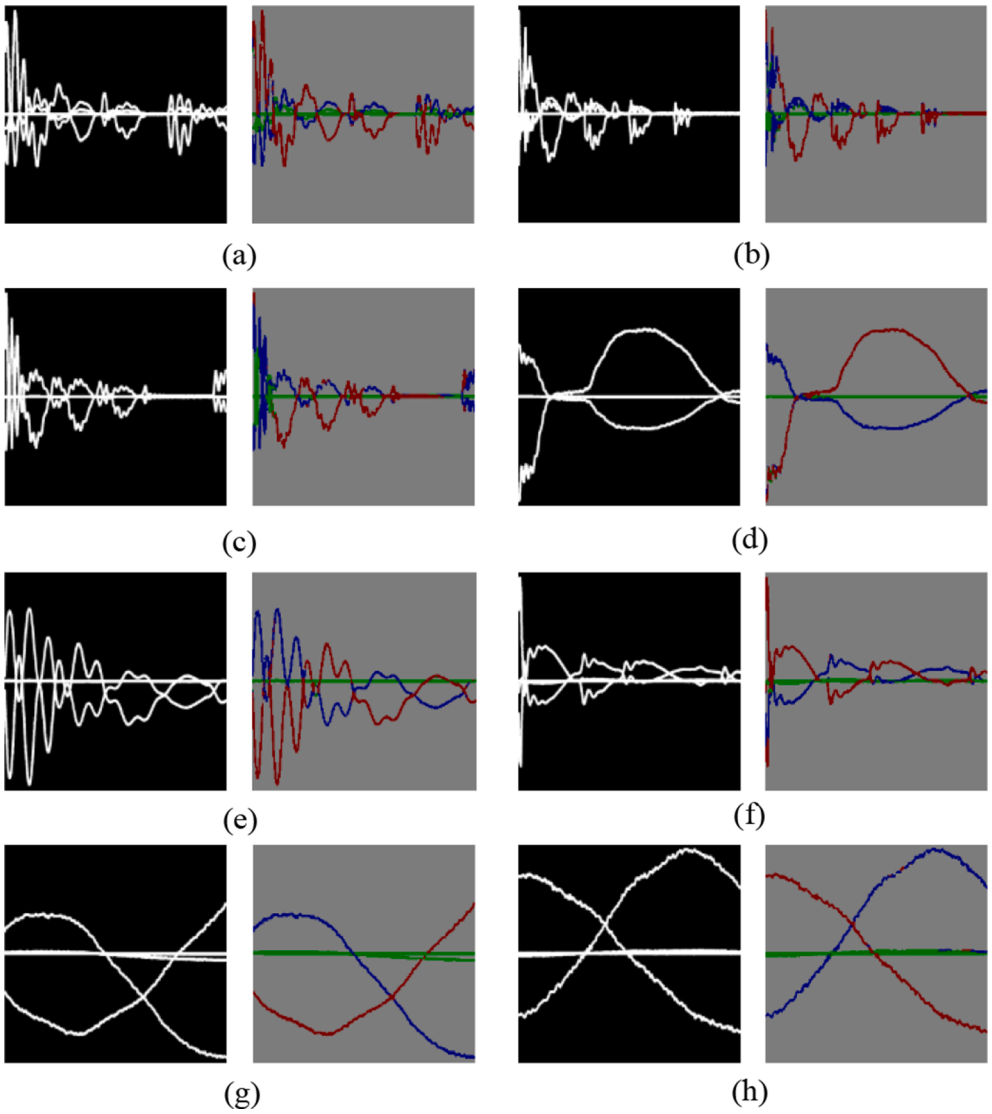

Fig. 11. Raw binary images and the corresponding segmentation results in field test (a) transient arc grounding fault in the ungrounded system; (b) arc grounding fault occurred in the cable line in the ungrounded system; (c) steady arc grounding fault in the ungrounded system; (d) single-phase line-broken fault; (e) transient arc grounding fault in the resonant grounding system; (f) arc grounding fault occurred in the cable line in the resonant grounding system; (g) SLG fault with 1000 Ω in the resonant grounding system; (h) SLG fault with 2000 Ω in the resonant grounding system.

Table 7
Detection accuracy in field test.

Grounding mode	Paper [26]	Paper [33]	Proposed method
Ungrounded	100%	×	**100%**
Resonant grounding	44.44%	100%	**100%**

distribution networks in Chenzhou and Shaoyang substations adopt the ungrounded mode, where 5 sets of fault data are collected, and the distribution network in Xi'an substation adopts the resonant grounding mode. Notably, different distribution networks have different feeder numbers, ranging from five to eight, and parameters, and the recorded SLG faults occurred under different fault conditions. Several binary images generated by the currents from practical distribution networks and the corresponding segmentation results are shown in Fig. 12, where the meanings of x-axis and y-axis are same as that in Fig. 7.

Evidently, it is relatively easy to distinguish the faulty feeder when SLG faults occurred in Chenzhou and Shaoyang substations. Whereas, the zero-sequence currents have noticeable distortions due to arc extinction and reignition in Xi'an substation. Meanwhile, there is a long time for the current to be zero when the arc is extinguished, which is significantly different from the currents in the training dataset. However, the proposed FCN can still effectively segment the waveform of the faulty feeder, and the corresponding dice coefficients are as follows: 0.91, 0.93, 0.92, 0.92, 0.62, 0.82, 0.86, and the dice coefficient of each feeder for the bus fault is smaller than 0.5.

The detection results are shown in Table 8. It can be seen that the method [33] has some misjudgments for faulty-feeder detection in the Xi'an substation. This is mainly because the calculated current amplitudes at the fundamental frequency and second-harmonic frequency are affected by arc grounding faults, and the threshold for distinguishing the bus fault and line fault may fail under these conditions. Furthermore, the method [26] would misjudge the bus fault as a line fault. In contrast, the proposed method has 100% detection accuracy in the practical distribution networks, which demonstrates its considerable application prospects.

5. Conclusion

Since the detection process cannot simultaneously satisfy completeness and interpretability, the existing faulty-feeder detection methods would have unacceptable performance under complex fault scenarios, such as small fault phase angles, high impedance grounding faults, and intermittent arc grounding faults. Specifically, the insufficiency of completeness would result in poor robustness, while the insufficiency of interpretability may lead to low application prospects. In addition, the physical meaning in the feature extraction process and

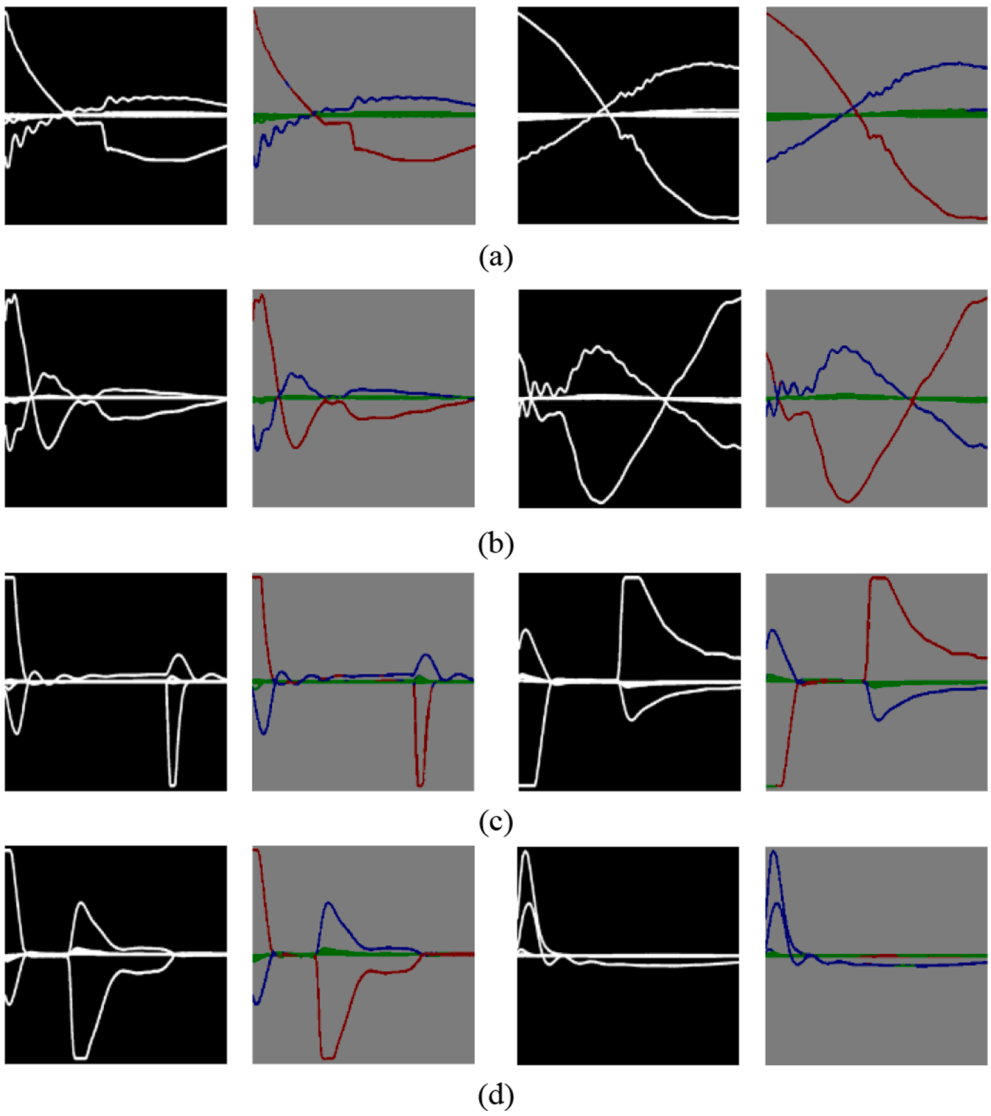

Fig. 12. Raw binary images and the corresponding segmentation results in the practical distribution networks (a) SLG faults occurred in Chenzhou substation; (b) SLG faults occurred in Shaoyang substation; (c) SLG faults occurred in Xi'an substation; (d) SLG faults occurred in Xi'an substation.

Table 8
Detection results in practical distribution networks.

Grounding mode	Paper [26]	Paper [33]	Proposed method
Ungrounded	100%	×	**100%**
Resonant grounding	85.71%	71.34%	**100%**

the efficiency of detection strategies also need to be further improved.

To solve these problems, this paper proposed an FCN-FTDE method, which seeks to enhance the physical meaning, completeness, interpretability, and detection strategy in detection process. The main conclusions are as follow:

1) The established FCN model can obtain waveforms with different meanings, which are segmented from the superimposed waveforms composed of all zero-sequence currents. The segmented waveforms have clear physical meaning and sufficient completeness, which corresponds to raw waveforms rather than specific fault characteristics.

2) The proposed FTDE method can evaluate the fault degree of each feeder on the waveform scale, which is calculated by comparing the segmented results to raw waveforms. The detection strategy is constructed based on the calculated dice coefficients, where the dice coefficient of the faulty feeder is larger than 0.5, and the detection process has good interpretability, which is simple, clear, intuitive, and effective.

3) Totally 13,237 sets of fault data are collected from PSCAD simulation, RTDS HIL test, field test, and practical distribution networks, and they are utilized to verify the detection performance of the proposed method. Large amounts of detection results show that the proposed method has 99.65% detection accuracy on average, and it can adapt to distribution networks with different topologies, varied parameters, high impedance grounding faults, and intermittent arc grounding faults, demonstrating its strong generalization capability and considerable application prospects.

CRediT authorship contribution statement

Jiawei Yuan: Conceptualization, Methodology, Software, Validation, Formal analysis, Investigation, Data curation, Writing – original draft, Writing – review & editing. **Zaibin Jiao:** Writing – original draft, Writing – review & editing, Supervision.

Declaration of Competing Interest

The authors declare that they have no known competing financial interests or personal relationships that could have appeared to influence

the work reported in this paper.

References

[1] Zeng X, Yu K, Wang Y, Xu Y. A novel single phase grounding fault protection scheme without threshold setting for neutral ineffectively earthed power systems. CSEE J Power Energy Syst 2016;2(3):73–81.

[2] Lin Y-H, Liu C-W, Chen C-S. A new PMU-based fault detection/location technique for transmission lines with consideration of arcing fault discrimination—part I: theory and algorithms. IEEE Trans Power Del 2004;19(4):1587–93.

[3] Huang W, Kaczmarek R. SLG fault detection in presence of strong capacitive currents in compensated networks. IEEE Trans Power Del 2007;22(4):2132–5.

[4] Jin N, Xing J, Liu Y, Li Z, Lin X. A novel Single-phase-to-ground fault identification and isolation strategy in wind farm collector line. Int J Elect Power Energy Syst 2018;94:15–26.

[5] Wang Y, Huang Y, Zeng X, Wei G, Zhou J, Fang T, et al. Faulty feeder detection of single phase-earth fault using grey relation degree in resonant grounding system. IEEE Trans Power Del 2017;32(1):55–61.

[6] Fan S, Xu B, Zhang Q. A new method for fault line selection in distribution system with ARC suppression coil grounding with square-wave signal injection. Automat Elect Power Syst 2012;36(4):91–5.

[7] Li Z, Ye Y, Ma X, Lin X, Xu F, Wang C, et al. Single-phase-to-ground fault section location in flexible resonant grounding distribution networks using soft open points. Int J Elect Power Energy Syst 2020;122:106198.

[8] Yuan J, Jiao Z, Feng G, Chen M, Xu M. Study on fault line detection methods based on multi-feature fusion in distribution systems. IET Gener Transm Distrib 2021;15(5):860–9.

[9] Cui T, Dong XZ. Hilbert-transform-based transient earth fault detection in non-effectively grounded distribution systems. IEEE Trans Power Del 2011;26(1):143–51.

[10] Kar S, Samantaray SR. Time-frequency transform-based differential scheme for microgrid protection. IET Gener Transm Distrib 2014;8(2):310–20.

[11] He Z, Fu L, Lin S, Bo Z. Fault detection and classification in EHV transmission line based on wavelet singular entropy. IEEE Trans Power Del 2010;25(4):2156–63.

[12] Lin C, Gao W, Guo M-F. Discrete wavelet transform-based triggering method for single-phase earth fault in power distribution systems. IEEE Trans Power Delivery 2019;34(5):2058–68.

[13] Gautam S, Brahma SM. Detection of high impedance fault in power distribution systems using mathematical morphology. IEEE Trans Power Syst 2013;28(2):1226–34.

[14] Namdari F, Salehi M. High-speed protection scheme based on initial current traveling wave for transmission lines employing mathematical morphology. IEEE Trans Power Del 2017;32(1):246–53.

[15] Dragomiretskiy K, Zosso D. Variational mode decomposition. IEEE Trans Signal Process 2014;62(3):531–44.

[16] Xie L, Luo L, Li Y, Zhang Yu, Cao Y. A traveling wave-based fault location method employing VMD-TEO for distribution network. IEEE Trans Power Delivery 2020;35(4):1987–98.

[17] Wang XW, et al. High impedance fault-detection method based on the variational mode decomposition and Teager-Kaiser energy operators for this distribution network. IEEE Trans Smart Grid 2019;10(6):6041–54.

[18] Guo M-F, Zeng X-D, Chen D-Y, Yang N-C. Deep-learning-based earth fault detection using continuous wavelet transform and convolutional neural network in resonant grounding distribution systems. IEEE Sens J 2018;18(3):1291–300.

[19] Zhai EJ, et al. Fault line selection method of small current grounding system based on VMD-LSTM. Adv Technol Electr Eng Energy 2021;40(1):70–80.

[20] Abdali A, Mazlumi K, Noroozian R. High-speed fault detection and location in DC microgrids systems using multi-criterion system and neural network. Appl Soft Comput 2019;79:341–53.

[21] Souza FAD, Castoldi MF, Goedtel A, Silva MD. A cascade perceptron and Kohonen network approach to fault location in rural distribution feeders. Appl Soft Comput 2020;96:106627.

[22] Guo M-F, Yang N-C. Features-clustering-based earth fault detection using singular-valuedecomposition and fuzzy c-means in resonant grounding distributionsystems. Int J Elect Power Energy Syst 2017;93:97–108.

[23] Yu K, Zou H, Zeng X, Li Y, Li H, Zhuo C, et al. Faulty feeder detection of single phase-earth fault based on fuzzy measure fusion criterion for distribution networks. Int J Electr Power Energy Syst 2021;125:106459.

[24] Chen K, et al. Fault line detection using sampled data processing and ADABOOST for small current grounding system. Proceed CSEE 2014;34(34):6228–37.

[25] Yuan JW, et al. Faulty feeder detection method for SLG faults in distribution networks based on comprehensive fault characteristics across entire frequency spectrum. Int J Elect Power Energy Syst 2022;140:107835.

[26] Wei X, Yang D, Wang X, Wang B, Gao J, Wei J. Faulty feeder detection based on fundamental component shift and multiple-transient-feature fusion in distribution networks. IEEE Trans Smart Grid 2021;12(2):1699–711.

[27] Xiaowei W, Xiangxiang W, Dechang Y, Guobing S, Jie G, Yanfang W, et al. Fault feeder detection method utilized steady state and transient components based on FFT backstepping in distribution networks. Int J Elect Power Energy Syst 2020;114:105391.

[28] Ghaderi A, Mohammadpour HA, Ginn HL, Shin Y. High impedance fault detection in the distribution network using the time frequency-based algorithm. IEEE Trans Power Del 2015;30(3):1260–8.

[29] Du Y, Liu Y, Shao Q, Luo L, Dai J, Sheng G, et al. Single line-to-ground faulted line detection of distribution systems with resonant grounding based on feature fusion framework. IEEE Trans Power Delivery 2019;34(4):1766–75.

[30] Yuan F, Zhang L, Xia X, Wan B, Huang Q, Li X. Deep smoke segmentation. Neurocomputing 2019;357:248–60.

[31] Long J, et al. Fully convolutional networks for semantic segmentation. In: Proceedings of the IEEE Conference on Computer Vision and Pattern Recognition; 2015. p. 3431–40.

[32] Lee CJ, Park JB, Shin JR, Radojevie ZM. A new two-terminal numerical algorithm for fault location, distance protection, and arcing fault recognition. IEEE Trans Power Syst 2006;21(3):1460–2.

[33] Liu P, Du S, Sun K, Zhu J, Xie D, Liu Y. Single-line-to-ground fault feeder selection considering device polarity reverse installation in resonant grounding system. IEEE Trans Power Delivery 2021;36(4):2204–12.